



# Ground-state properties of ${}^4\text{He}$ and ${}^{16}\text{O}$ extrapolated from lattice QCD with pionless EFT



L. Contessi<sup>a,b</sup>, A. Lovato<sup>c</sup>, F. Pederiva<sup>a,b,\*</sup>, A. Roggero<sup>d</sup>, J. Kirscher<sup>e</sup>, U. van Kolck<sup>f,g</sup>

<sup>a</sup> Physics Department, University of Trento, Via Sommarive 14, I-38123 Trento, Italy

<sup>b</sup> INFN-TIFPA Trento Institute of Fundamental Physics and Applications, Via Sommarive, 14, 38123 Povo TN, Italy

<sup>c</sup> Physics Division, Argonne National Laboratory, Argonne, IL 60439, USA

<sup>d</sup> Institute for Nuclear Theory, University of Washington, Seattle, WA 98195, USA

<sup>e</sup> Department of Physics, The City College of New York, New York, NY 10031, USA

<sup>f</sup> Institut de Physique Nucléaire, CNRS/IN2P3, Univ. Paris-Sud, Université Paris-Saclay, F-91406 Orsay, France

<sup>g</sup> Department of Physics, University of Arizona, Tucson, AZ 85721, USA

## ARTICLE INFO

### Article history:

Received 25 January 2017

Received in revised form 8 May 2017

Accepted 24 July 2017

Available online 26 July 2017

Editor: W. Haxton

## ABSTRACT

We extend the prediction range of Pionless Effective Field Theory with an analysis of the ground state of  ${}^{16}\text{O}$  in leading order. To renormalize the theory, we use as input both experimental data and lattice QCD predictions of nuclear observables, which probe the sensitivity of nuclei to increased quark masses. The nuclear many-body Schrödinger equation is solved with the Auxiliary Field Diffusion Monte Carlo method. For the first time in a nuclear quantum Monte Carlo calculation, a linear optimization procedure, which allows us to devise an accurate trial wave function with a large number of variational parameters, is adopted. The method yields a binding energy of  ${}^4\text{He}$  which is in good agreement with experiment at physical pion mass and with lattice calculations at larger pion masses. At leading order we do not find any evidence of a  ${}^{16}\text{O}$  state which is stable against breakup into four  ${}^4\text{He}$ , although higher-order terms could bind  ${}^{16}\text{O}$ .

© 2017 The Authors. Published by Elsevier B.V. This is an open access article under the CC BY license (<http://creativecommons.org/licenses/by/4.0/>). Funded by SCOAP<sup>3</sup>.

## 1. Introduction

Establishing a clear path leading from the fundamental theory of strong interactions, namely Quantum Chromodynamics (QCD), to nuclear observables, such as nuclear masses and electroweak transitions, is one of the main goals of modern nuclear theory. At present, the most reliable numerical technique to perform QCD calculations is Lattice QCD (LQCD). It combines recent advances in high-performance computing, innovative algorithms, and conceptual breakthroughs in nuclear theory to produce predictions of nucleon–nucleon scattering, and the binding energies and magnetic moments of light nuclei. However, there are technical problems, which have so far limited the applicability of LQCD to  $A \leq 4$  baryon systems and to artificially large quark masses. Then, LQCD calculations require significantly smaller computational resources to yield meaningful signal-to-noise ratios. In this paper, we consider as examples LQCD data sets comprised of binding ener-

gies obtained at pion masses of  $m_\pi \simeq 805$  MeV [1] and  $m_\pi \simeq 510$  MeV [2].

The link between QCD and the entire nuclear landscape is a Hamiltonian whose systematic derivation was developed in the framework of effective field theory (EFT) in the last two decades [3–5]. This is achieved by exploiting a separation between “hard” ( $M$ ) and “soft” ( $Q$ ) momentum scales. The active degrees of freedom at soft scales are hadrons whose interactions are consistent with QCD. Effective potentials and currents are derived from the most general Lagrangian constrained by the QCD symmetries, and employed with standard few- and many-body techniques to make predictions for nuclear observables in a systematic expansion in  $Q/M$ . The interaction strengths carry information about the details of the QCD dynamics, and can be obtained by matching observables calculated in EFT and LQCD.

The aim of this work is the first extension of this program to the realm of medium-heavy nuclei. By using Pionless EFT (EFT( $\pi$ )) coupled to the Auxiliary Field Diffusion Monte Carlo (AFDMC) method [6] we analyze the connection between the ground state of  ${}^{16}\text{O}$  and its nucleon constituents. Beside physical data, the consideration of higher quark-mass input allows us to investigate the

\* Corresponding author.

E-mail address: [francesco.pederiva@unitn.it](mailto:francesco.pederiva@unitn.it) (F. Pederiva).

sensitivity of  $^{16}\text{O}$  stability to the pion mass. The usefulness of EFT( $\mathcal{N}$ ) [3,4] for the analysis of LQCD calculations has been discussed previously [7–9].

Whether EFT( $\mathcal{N}$ ) can be extended to real and lattice nuclei in the medium-mass region is an open question. For physical pion mass, convergence has been demonstrated in leading orders for the low-energy properties of  $A = 2, 3$  systems [10–14]. Counterintuitively, the binding energy of the  $A = 4$  ground state was found in good agreement with experiment at leading order (LO) [15], and even the  $A = 6$  ground state comes out reasonably well at this order [16]. A similar binding energy per nucleon for  $^4\text{He}$  ( $\simeq 7$  MeV) and  $^{16}\text{O}$  ( $\simeq 8$  MeV) suggests that EFT( $\mathcal{N}$ ) might converge for heavier systems. However, the difference in total binding energy between the two systems is quite large. Moreover, many-body effects become stronger, and quantum correlations might substantially change the picture. We chose  $^{16}\text{O}$  for mainly two reasons: First, because it is a doubly magic nucleus, thereby reducing the technical difficulties related to the construction of wave functions with the correct quantum numbers and symmetries. Second, its central density is sufficiently high to probe saturation properties and thereby serve as a model for even heavier nuclei.

In this first calculation of an  $A > 6$  system in EFT( $\mathcal{N}$ ) we work at LO. While the error of an LO calculation is relatively large (expected to be about 30%), it still allows us to exclude a catastrophic failure of saturation in this EFT. Our predictions for  $^4\text{He}$  and  $^{16}\text{O}$  use as input only the properties of the deuteron, dineutron and triton, and are consistent with renormalization-group invariance. We find that the ground state energy of 16 nucleons is indistinguishable from the four- $^4\text{He}$  threshold at all values of quark masses we consider. At physical pion mass the experimental  $^{16}\text{O}$  binding energy is within the EFT truncation error, being potentially reachable in higher orders. Thus, we can conclude that EFT( $\mathcal{N}$ ) has the elements needed for saturation, and we provide a baseline against which the convergence of EFT( $\mathcal{N}$ ) in medium-mass nuclei can be judged in future higher-order calculations. At this point, because of their complexity, strictly perturbative NLO and  $\text{N}^2\text{LO}$  calculations have been limited to  $A = 2, 3$  [10–14].

Using LQCD data as input enables the study of the nuclear chart as a function of the quark masses. We employ the standard method of determining EFT parameters theoretically, that of “matching” observables calculated in EFT to the same observables calculated in the underlying theory [17,18]. Operationally, fitting EFT parameters to LQCD data is not different than fitting them to experimental data. In contrast, conceptually it means that the resulting EFT predictions are consequences of QCD itself. When experimental data are fitted instead, the corresponding EFT predictions are consequences of any underlying theory that shares the symmetries of QCD.

At present there is no LQCD data for light nuclei at physical quark masses, so in this case we use experimental data as input. There is also no consensus about how binding energies behave as quark masses increase, with different lattice approaches yielding contradictory results. We use data [1,2] obtained from the identification of plateaus in the imaginary-time evolution within a box. This identification has been subject to criticism [19]. For  $A = 2$ , an independent analysis of the same data [1] yields different binding energies [20]. For different gauge configurations, a method based on the extraction (under certain assumptions) of a potential finds no bound states [21]. Our input should thus be seen as illustrative. However, as shown before [7,9] and confirmed here, the  $^4\text{He}$  binding energy predicted by LO EFT( $\mathcal{N}$ ) does agree with that found in Refs. [1,2]. Although the large errors do not allow a definitive conclusion, this coincidence is suggestive of a consistent plateau identification. It also supports the validity of EFT( $\mathcal{N}$ ).

In practice, our calculation is carried out as follows. In order to show renormalizability, we use potentials characterized by cutoffs up to  $\simeq 1.5$  GeV. This introduces non-trivial difficulties in solving the Schrödinger equation due to the rapidly changing behavior of the wave functions. To this aim, we developed an efficient linear optimization scheme to devise high-quality variational wave functions. Those have been employed as a starting point for the imaginary-time projection of AFDMC which enhances the ground-state component of the trial wave function. Finally, to alleviate the sign problem, we have also performed unconstrained propagations and studied their convergence pattern. We show that, thanks to these developments, the errors from the AFDMC calculation are now much smaller than the uncertainty originating from the EFT( $\mathcal{N}$ ) truncation and the LQCD input. The door is open for higher-order calculations with future, more precise LQCD input.

The rest of the paper is organized as follows: in Sec. 2 we will briefly review the properties of EFT( $\mathcal{N}$ ) that are relevant for our discussion; in Sec. 3 the methodological aspect of the calculations will be discussed; in Sec. 4 we will present and discuss our results; and finally Sec. 5 is devoted to conclusions. An appendix describes the way we estimate errors.

## 2. Pionless effective field theory

The relativistic, underlying theory, which presumably allows for the description of nuclei from first principles, is QCD. Low-energy processes in nuclear physics involve small enough momenta to justify the use of a nonrelativistic approach. Consequently, nucleon number is conserved and nuclear dynamics can be described within nonrelativistic many-body theory, while the strong nuclear potential needs to include only parity and time-reversal conserving operators. All relativistic corrections are sub-leading.

In this paper we are interested in the ground states of nuclei. The characteristic momentum in a two-body bound state of binding energy  $B_2$  is given by the location of the pole of the  $S$  matrix in the complex momentum plane,  $Q_2 = \sqrt{m_N B_2}$ , where  $m_N$  is the nucleon mass. To our knowledge, there is no consensus for a definition of an analogous characteristic momentum for larger nuclei bound by  $B_A$ ; as an estimate one can use a generalization where each nucleon contributes equally,

$$Q_A = \sqrt{2m_N \frac{B_A}{A}}. \quad (1)$$

For lattice  $^4\text{He}$  at  $m_\pi = 805$  MeV ( $m_\pi = 510$  MeV), where  $B_4 \simeq 110$  MeV [1] ( $B_4 \simeq 40$  MeV [2]) with  $m_N \simeq 1600$  MeV ( $m_N \simeq 1300$  MeV), this estimate gives  $Q_4/m_\pi \simeq 0.4$  (0.3). Thus, the typical momentum is small in comparison not only with  $m_N$ , but also with  $m_\pi$ , allowing for a description where pion exchanges are treated as unresolved contact interactions. The case is less clear-cut in the real world, where  $Q_4/m_\pi \simeq 0.8$ , but LO results [15] suggest that Eq. (1) overestimates the typical momentum. In fact, a similar inference can be made from results of the analog of EFT( $\mathcal{N}$ ) for  $^4\text{He}$  atomic clusters [22]. At physical  $m_\pi$ , the binding energy per particle in  $^{16}\text{O}$  is similar to that in  $^4\text{He}$ , so EFT( $\mathcal{N}$ ) might converge for this nucleus as well.

With pions integrated out,  $m_\pi$  gives an upper bound on the breakdown scale  $M$  of the EFT. The momentum associated with nucleon excitations of mass  $m_R$  is given by Eq. (1) with  $B_A/A \rightarrow m_R - m_N$ . For the lightest excitation, the Delta isobar,  $m_\Delta - m_N$  decreases as  $m_\pi$  increases. For  $m_\pi = 805$  MeV,  $\sqrt{2m_N(m_\Delta - m_N)}$  becomes comparable to  $m_\pi$ . Thus, throughout the considered range of pion masses nucleon resonances can also be treated as short-range effects, and nucleons are indeed the only relevant degrees of freedom.

The most general Lagrangian compatible with the symmetries of QCD consists, at leading order in  $1/M$ , of the nucleon kinetic term, two two-nucleon contact interactions, and one three-nucleon contact interaction. The singularity of these interactions leads to divergences that need to be dealt with by regularization and renormalization. Here, as in Refs. [7,9], we use a Gaussian regulator that suppresses transferred momenta above an ultraviolet cutoff  $\Lambda$ . This choice ensures that the Lagrangian can be transformed into a Hamiltonian containing only local potentials, suitable to be used within AFDMC. The Hamiltonian in coordinate space reads [7,9]

$$H_{LO} = - \sum_i \frac{\vec{\nabla}_i^2}{2m_N} + \sum_{i<j} (C_1 + C_2 \vec{\sigma}_i \cdot \vec{\sigma}_j) e^{-r_{ij}^2 \Lambda^2/4} + D_0 \sum_{i<j<k} \sum_{\text{cyc}} e^{-(r_{ik}^2 + r_{ij}^2) \Lambda^2/4}, \quad (2)$$

where the sums are over, respectively, nucleons, nucleon pairs, and nucleon triplets, and  $\sum_{\text{cyc}}$  stands for the cyclic permutation of  $i$ ,  $j$ , and  $k$ . Dependence on the arbitrary regulator choice is eliminated by allowing the interaction strengths, or low-energy constants (LECs),  $C_1(\Lambda)$ ,  $C_2(\Lambda)$  and  $D_0(\Lambda)$  to depend on  $\Lambda$ .

To solve the two-nucleon system, in principle one iterates interactions only in the channels containing  $S$ -matrix poles within the convergence range of the theory [23]. Since two nucleons have a bound state in the  $^3S_1$  channel and a shallow virtual state (which becomes a bound state as  $m_\pi$  increases [1,2]) in the  $^1S_0$  channel, one needs to include two interactions at LO and treat them non-perturbatively. In Eq. (2) we chose the operator basis 1 and  $\vec{\sigma}_i \cdot \vec{\sigma}_j$ , but it can be replaced by any other form equivalent under Fierz transformations in  $SU(2)$ . All these possible choices are equally convenient for an AFDMC calculation.

When the three-body problem is solved with these interactions, renormalizability requires a contact three-nucleon force at LO [24]. As for the two-body interactions, there is some freedom in choosing the operator to include in the Hamiltonian formulation of the three-body force. For simplicity we use a central potential, which makes obvious the Wigner spin–isospin symmetry ( $SU(4)$ ) of this force.

For renormalization at LO, we ensure that three uncorrelated observables are  $\Lambda$ -independent. Here we follow Ref. [9] and choose these observables as the deuteron and triton binding energies and, for physical (unphysical) pion mass(es) the  $^1S_0$  scattering length (dineutron binding energy). The LECs' dependence on the cutoff can be found in Ref. [9]. In particular, because  $C_1(\Lambda) \gg C_2(\Lambda)$ , the LO Hamiltonian has an approximate  $SU(4)$  symmetry.

Interactions with more derivatives represent higher orders. For example, at NLO the first two-body energy corrections appear in the form of two-derivative contact interactions [23]. For ground states electromagnetic interactions are also sub-leading, starting at NLO with the Coulomb interaction [13]. Since sub-leading interactions are suppressed by powers of  $M$ , they should be included as perturbations. Treating them non-perturbatively, like the LO terms, is problematic as the iteration of sub-leading terms usually destroys renormalizability. NLO interactions have been dealt with fully perturbatively only for  $A = 2$  [10,11] and  $A = 3$  [12,13]. Given the challenges posed by such calculations, we limit ourselves to LO in this first foray into medium-mass nuclei.

One feature of the EFT approach is a better understanding of the systematic uncertainties which reduce the accuracy of predicted nuclear observables. Apart from the errors germane to AFDMC, the EFT at LO is expected to be affected by systematic, relative errors of  $O(Q_A/M, Q_A/\Lambda)$  plus “measurement” uncertainties in the LECs.

For observables that were not used as input, regularization introduces an error proportional to the inverse of the cutoff. For example, different Fierz-reordered forms of the potential only give the same results for large cutoffs. In order to minimize the regularization error, we fit finite-cutoff results with

$$O_\Lambda = O + \frac{C_0}{\Lambda} + \frac{C_1}{\Lambda^2} + \dots, \quad (3)$$

where  $O$  is the observable at  $\Lambda \rightarrow \infty$ , while the parameters  $C_0, C_1, \dots$ , are specific for each observable. The number of powers of  $\Lambda$  needed to perform a meaningful extrapolation is not known *a priori*. The standard prescription consists in truncating the expansion when adding additional powers of  $1/\Lambda$  no longer influences  $O$ . In a renormalizable theory, observables converge in the  $\Lambda \rightarrow \infty$  limit to a value that must not be confused with a precise physical result. Observables are unavoidably plagued by the truncation error, which cannot be reduced without a next-order calculation.

The truncation of a natural EFT expansion at order  $n$  allows for a residual error proportional to  $(Q/M)^{n+1}$ , where the constant of proportionality depends on the specific observable. Truncation errors are more difficult to assess here because the scales  $M$  and  $Q_A$  are not well known. Assuming  $M \sim m_\pi$  and  $Q_A \sim Q_{3,4}$ , as given in Eq. (1), one estimates  $Q_A/M \sim 1/3$  for physical quarks. An alternative that does not rely on an estimate for  $Q_A$  uses cutoff variation to place a lower bound on the truncation error. The residual cutoff dependence cannot be distinguished from higher-order contributions. Assuming that for the observable of interest the leading missing power of  $1/M$  is the same as the leading power of  $1/\Lambda$ , varying  $\Lambda$  from  $M$  to much larger values gives an estimate of the truncation error. For another technique to estimate the EFT truncation error, see for example Ref. [25].

Finally, experimental and numerical LQCD uncertainties are transcribed through the renormalization of the LECs. While this is not an important issue for the physical data, LQCD “measurements” carry a significant uncertainty which could dramatically affect EFT predictions. Estimating their effects would require a huge computational effort, as the calculation would have to be repeated for various combinations of the extreme values the LECs can take. Since the pertinent errors [1,2] are comparable to the LO truncation error, this effort is not yet justified. We will limit ourselves to show that the Monte Carlo errors discussed in the next section have reached a point where they are not an obstacle to future higher-order calculations. At that point, a more detailed analysis of the propagation of “measurement” errors at unphysical pion masses will be required.

### 3. Monte Carlo method

Quantum Monte Carlo (QMC) methods allow for solving the time-independent Schrödinger equation of a many-body system, providing an accurate estimate of the statistical error of the calculation. For light nuclei, QMC and, in particular, Green's Function Monte Carlo (GFMC) methods have been successfully exploited to carry out calculations of nuclear properties, based on realistic Hamiltonians including two- and three-nucleon potentials, and consistent one- and two-body meson-exchange currents [26].

Because the GFMC method involves a sum over spin and isospin, its computational requirements grow exponentially with the number of particles. Over the past two decades AFDMC [6] has emerged as a more efficient algorithm for dealing with larger nuclear systems [27], but only for somewhat simplified interactions. Within AFDMC, the spin–isospin degrees of freedom are described by single-particle spinors, the amplitudes of which are sampled using Monte Carlo techniques, and the coordinate-space diffusion in

GFMC is extended to include diffusion in spin and isospin spaces. Both GFMC and AFDMC have no difficulties in using realistic two- and three-body forces; the interactions are not required to be soft and hence can generate wave functions with high-momentum components. This is particularly relevant to analyze the cutoff dependence of observables, as relatively large values for  $\Lambda$  are to be considered in order to confirm renormalizability.

QMC methods employ an imaginary-time ( $\tau$ ) propagation in order to extract the lowest many-body state  $\Psi_0$  from a given initial trial wave function  $\Psi_T$ :

$$|\Psi_0\rangle = \lim_{\tau \rightarrow \infty} e^{-(H-E_T)\tau} |\Psi_T\rangle. \quad (4)$$

In the above equation  $E_T$  is a parameter that controls the normalization of the wave function and  $H$  is the Hamiltonian of the system. In order to efficiently deal with spin–isospin dependent Hamiltonians, the Hubbard–Stratonovich transformation is applied to the quadratic spin and isospin operators entering the imaginary-time propagator to make them linear. As a consequence, the computational cost of the calculation is reduced from exponential to polynomial in the number of particles, allowing for the study of many-nucleon systems.

The standard form of the wave function used in QMC calculations of light nuclei reads

$$\langle X|\Psi_T\rangle = \langle X|\left(\prod_{i<j<k} U_{ijk}\right)\left(\prod_{i<j} F_{ij}\right)|\Phi\rangle, \quad (5)$$

where  $X = \{x_1 \dots x_A\}$  and the generalized coordinate  $x_i = \{r_i, \sigma_i, \tau_i\}$  represents the position, spin, and isospin variables of the  $i$ -th nucleon. The long-range behavior of the wave function is described by the Slater determinant

$$\langle X|\Phi\rangle = \mathcal{A}\{\phi_{\alpha_1}(x_1), \dots, \phi_{\alpha_A}(x_A)\}. \quad (6)$$

The symbol  $\mathcal{A}$  denotes the antisymmetrization operator and  $\alpha$  denotes the quantum numbers of the single-particle orbitals, given by

$$\phi_{\alpha}(x) = R_{nl}(r) Y_{\ell\ell_z}(\hat{r}) \chi_{ss_z}(\sigma) \chi_{\tau\tau_z}(\tau), \quad (7)$$

where  $R_{nl}(r)$  is the radial function,  $Y_{\ell\ell_z}(\hat{r})$  is the spherical harmonic, and  $\chi_{ss_z}(\sigma)$  and  $\chi_{\tau\tau_z}(\tau)$  are the complex spinors describing the spin and isospin of the single-particle state.

In both the GFMC and the latest AFDMC calculations spin–isospin dependent correlations  $F_{ij}$  and  $U_{ijk}$  are usually adopted. However, these are not necessary for this work. In fact, the two-body LO pionless nuclear potential considered in this work does not contain tensor or spin-orbit operators. In addition, the LEC proportional to the spin-dependent component of the interaction is much smaller than the one of the central channel,  $C_2 \ll C_1$ . Finally, Fierz transformations allow us to consider the purely central three-body force in Eq. (2). As a consequence, we can limit ourselves to spin–isospin independent two- and three-body correlations only,

$$F_{ij} = f(r_{ij}), \quad (8)$$

$$U_{ijk} = 1 - \sum_{\text{cyc}} [u(r_{ij})u(r_{jk}) + u(r_{ij})u(r_{ik}) + u(r_{ik})u(r_{jk})], \quad (9)$$

where  $f(r)$  and  $u(r)$  are functions of the radius only.

The radial functions of the orbitals as well as those entering the two- and three-body Jastrow correlations are determined minimizing the ground-state expectation value of the Hamiltonian,

$$E_V = \frac{\langle \Psi_T | H | \Psi_T \rangle}{\langle \Psi_T | \Psi_T \rangle}. \quad (10)$$

In standard nuclear Variational Monte Carlo (VMC) and GFMC calculations the minimization is usually done adopting a “hand-waving” procedure, while in more recent AFDMC calculations the stochastic reconfiguration (SR) method [28] has been adopted. In both cases the number of variational parameters is reduced by first minimizing the two-body cluster contribution to the energy per particle, as described in Refs. [29,30]. In this work we adopt, for the first time in a nuclear QMC calculation, the more advanced *linear method* (LM) [31], which allows us to deal with a much larger number of variational parameters.

Within the LM, at each optimization step we expand the normalized trial wave function

$$|\tilde{\Psi}_T(\mathbf{p})\rangle = \frac{|\Psi_T(\mathbf{p})\rangle}{\sqrt{\langle \Psi_T(\mathbf{p}) | \Psi_T(\mathbf{p}) \rangle}} \quad (11)$$

at first order around the current set of variational parameters  $\mathbf{p}^0 = \{p_1^0, \dots, p_{N_p}^0\}$ ,

$$|\tilde{\Psi}_T^{\text{lin}}(\mathbf{p})\rangle = |\tilde{\Psi}_T(\mathbf{p}^0)\rangle + \sum_{i=1}^{N_p} \Delta p_i |\tilde{\Psi}_T^i(\mathbf{p}^0)\rangle. \quad (12)$$

By imposing  $\langle \Psi_T(\mathbf{p}^0) | \tilde{\Psi}_T(\mathbf{p}^0) \rangle = 1$ , we ensure that

$$\begin{aligned} |\tilde{\Psi}_T^i(\mathbf{p}^0)\rangle &= \left. \frac{\partial |\tilde{\Psi}_T(\mathbf{p})\rangle}{\partial p_i} \right|_{\mathbf{p}=\mathbf{p}^0} \\ &= |\Psi_T^i(\mathbf{p}^0)\rangle - S_{0i} |\Psi_T(\mathbf{p}^0)\rangle \end{aligned} \quad (13)$$

are orthogonal to  $|\Psi_T(\mathbf{p}^0)\rangle$ . In the last equation we have introduced

$$|\Psi_T^i(\mathbf{p}^0)\rangle = \left. \frac{\partial |\Psi_T(\mathbf{p})\rangle}{\partial p_i} \right|_{\mathbf{p}=\mathbf{p}^0} \quad (14)$$

for the first derivative with respect to the  $i$ -th parameter, and the overlap matrix is defined by  $S_{0i} = \langle \Psi_T(\mathbf{p}^0) | \Psi_T^i(\mathbf{p}^0) \rangle$ . The expectation value of the energy on the linear wave function is defined as

$$E_{\text{lin}}(\mathbf{p}) \equiv \frac{\langle \tilde{\Psi}_T^{\text{lin}}(\mathbf{p}) | H | \tilde{\Psi}_T^{\text{lin}}(\mathbf{p}) \rangle}{\langle \tilde{\Psi}_T^{\text{lin}}(\mathbf{p}) | \tilde{\Psi}_T^{\text{lin}}(\mathbf{p}) \rangle}. \quad (15)$$

The variation  $\Delta \tilde{\mathbf{p}}$  of the parameters that minimizes the energy,  $\nabla_{\mathbf{p}} E_{\text{lin}}(\mathbf{p}) = 0$ , corresponds to the lowest eigenvalue solution of the generalized eigenvalue equation

$$\tilde{H} \Delta \mathbf{p} = \Delta E \tilde{S} \Delta \mathbf{p}, \quad (16)$$

where  $\tilde{H}$  and  $\tilde{S}$  are the Hamiltonian and overlap matrices in the  $(N_p + 1)$ -dimensional basis defined by  $\{|\tilde{\Psi}_T(\mathbf{p}^0)\rangle, |\tilde{\Psi}_T^1(\mathbf{p}^0)\rangle, \dots, |\tilde{\Psi}_T^{N_p}(\mathbf{p}^0)\rangle\}$ . The authors of Ref. [32] have shown that writing the expectation values of these matrix elements in terms of covariances allows us to keep their statistical error under control even when they are estimated over a relatively small Monte Carlo sample. However, since in AFDMC the derivatives of the wave function with respect to the orbital variational parameters are in general complex, we generalized the expressions for the estimators reported in the appendix of Ref. [32].

For a finite sample size the matrix  $\tilde{H}$  can be ill-conditioned, spoiling therefore the numerical inversion needed to solve the eigenvalue problem. A practical procedure to stabilize the algorithm is to add a small positive constant  $\epsilon$  to the diagonal matrix elements of  $\tilde{H}$  except for the first one,  $\tilde{H}_{ij} \rightarrow \tilde{H}_{ij} + \epsilon(1 - \delta_{i0})\delta_{ij}$ . This procedure reduces the length of  $\Delta \tilde{\mathbf{p}}$  and rotates it towards the steepest-descent direction.

It has to be noted that if the wave function depends linearly upon the variational parameters, the algorithm converges in just one iteration. However, in our case strong nonlinearities in the

variational parameters make, in some instances,  $|\bar{\Psi}_T^{\text{lin}}(\mathbf{p})\rangle$  significantly different from  $|\bar{\Psi}_T(\mathbf{p}^0 + \Delta\mathbf{p})\rangle$ . Accounting for the quadratic term in the expansion as in the Newton method [33,32] would alleviate the problem, at the expense of having to estimate also the Hessian of the wave function with respect to the variational parameters. An alternative strategy consists in taking advantage of the arbitrariness of the wave-function normalization to improve on the convergence by a suitable rescaling of the parameter variation [32,31]. We found that this procedure was not sufficient to guarantee the stability of the minimization procedure. For this reason we have implemented the following heuristic procedure. For a given value of  $\epsilon$ , Eq. (16) is solved. If the linear variation of the wave function for  $\mathbf{p} = \mathbf{p}^0 + \Delta\mathbf{p}$  is small,

$$\frac{|\bar{\Psi}_T^{\text{lin}}(\mathbf{p})|^2}{|\bar{\Psi}_T(\mathbf{p}^0)|^2} = 1 + \sum_{i,j=1}^{N_p} \bar{S}_{ij} \Delta p^i \Delta p^j \leq \delta, \quad (17)$$

a short correlated run is performed in which the energy expectation value

$$E(\mathbf{p}) \equiv \frac{\langle \bar{\Psi}_T(\mathbf{p}) | H | \bar{\Psi}_T(\mathbf{p}) \rangle}{\langle \bar{\Psi}_T(\mathbf{p}) | \bar{\Psi}_T(\mathbf{p}) \rangle} \quad (18)$$

is estimated along with the full variation of the wave function for a set of possible values of  $\epsilon$  (in our case  $\approx 100$  values are considered). The optimal  $\epsilon$  is chosen so as to minimize  $E(\bar{\mathbf{p}})$  provided that

$$\frac{|\bar{\Psi}_T(\bar{\mathbf{p}})|^2}{|\bar{\Psi}_T(\mathbf{p}^0)|^2} \leq \delta. \quad (19)$$

Note that, at variance with the previous expression, here in the numerator we have the full wave function instead of its linearized approximation. In the (rare) cases where no acceptable value of  $\epsilon$  is found due to possibly large statistical fluctuations in the VMC estimators, we perform an additional run adopting the previous parameter set and a new optimization is attempted. In our experience, this procedure proved extremely robust.

The chief advantage of the additional constraint is that it suppresses the potential instabilities caused by the nonlinear dependence of the wave function on the variational parameters. When using the “standard” version of the LM, there were instances in which, despite the variation of the linear wave function being well below the threshold of Eq. (17), the full wave function fluctuated significantly more, preventing the convergence of the minimization algorithm. As for the wave-function variation, we found that choosing  $\delta = 0.2$  guarantees a fast and stable convergence.

The two-body Jastrow correlation  $f(r_{ij})$  is written in terms of cubic splines, characterized by a smooth first derivative and continuous second derivative. The adjustable parameters to be optimized are the “knots” of the spline, which are simply the values of the Jastrow function at the grid points, and the value of the first derivative at  $r_{ij} = 0$ . Analogous parametrizations are adopted for  $u(r_{ij})$  and  $R_{n\ell}(r_i)$ . In the  ${}^4\text{He}$  case we used six variational parameters for  $f(r)$ ,  $u(r)$ , and for the radial orbital functions  $R_{n\ell}(r)$ . This allowed enough flexibility for the variational energies to be very close to the one obtained performing the imaginary-time diffusion for all values of the cutoff and of the pion mass. On the other hand, to allow for an emerging cluster structure, for the  ${}^{16}\text{O}$  wave function we used 30 parameters for the two- and three-body Jastrow correlations and 15 parameters for each of the  $R_{n\ell}(r)$ .

The LM exhibits a much faster convergence pattern than the SR, previously used in AFDMC. In Fig. 1, we show the  ${}^4\text{He}$  variational energy obtained for physical pion mass and  $\Lambda = 4 \text{ fm}^{-1}$  as a function of the number of optimization steps for both SR and LM. While the LM takes only  $\simeq 15$  steps to converge, the SR is much

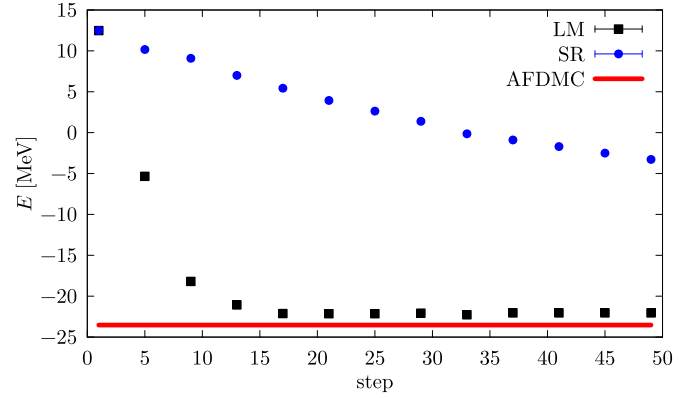


**Fig. 1.** (Color online) Convergence pattern of the  ${}^4\text{He}$  variational energy at physical pion mass and  $\Lambda = 4 \text{ fm}^{-1}$  as a function of the number of optimization steps for the LM method (black squares) and the SR (blue circles). For comparison, the red line indicates the AFDMC result.

**Table 1**

${}^4\text{He}$  energy for different values of the pion mass  $m_\pi$  and the cutoff  $\Lambda$ , compared to experiment and LQCD calculations [1,2]. See main text and appendix for details on errors and extrapolations.

$\Lambda$	$m_\pi = 140 \text{ MeV}$	$m_\pi = 510 \text{ MeV}$	$m_\pi = 805 \text{ MeV}$
$2 \text{ fm}^{-1}$	$-23.17 \pm 0.02$	$-31.15 \pm 0.02$	$-88.09 \pm 0.01$
$4 \text{ fm}^{-1}$	$-23.63 \pm 0.03$	$-34.88 \pm 0.03$	$-91.40 \pm 0.03$
$6 \text{ fm}^{-1}$	$-25.06 \pm 0.02$	$-36.89 \pm 0.02$	$-96.97 \pm 0.01$
$8 \text{ fm}^{-1}$	$-26.04 \pm 0.05$	$-37.65 \pm 0.03$	$-101.72 \pm 0.03$
$\rightarrow \infty$	$-30_{\pm 2}^{\pm 0.3(\text{sys})}$	$-39_{\pm 2}^{\pm 1(\text{sys})}$	$-124_{\pm 1}^{\pm 3(\text{sys})}$
Exp.	$-28.30$	–	–
LQCD	–	$-43.0 \pm 14.4$	$-107.0 \pm 24.2$

slower; after 50 steps the energy is still much above the asymptotic limit. We have observed analogous behavior for other values of the cutoff and the pion mass. In the  ${}^{16}\text{O}$  case, the improvement of the LM with respect to the SR is even more dramatic due to the clustering of the wave function, which will be discussed in detail in the following.

## 4. Results

With LO EFT( $\mathcal{N}$ ) LECs determined from experiment or LQCD calculations, predictions can be made with AFDMC for the binding energies of  ${}^4\text{He}$  and  ${}^{16}\text{O}$ .

In Table 1 we report results of  ${}^4\text{He}$  energies for all the values of the cutoff and of the pion mass we considered. Despite the different parametrization of the variational wave functions, the results are in very good agreement with those reported in Ref. [7], where a simplified version of the variational wave function was used because the LM had not been introduced yet. For most cutoff values, our results also agree with those of Ref. [9], which were obtained with the Resonating-Group and Hyperspherical-Harmonic methods. For  $\Lambda \leq 6 \text{ fm}^{-1}$ , the QMC results differ by less than 0.1 MeV from Ref. [9], while for  $\Lambda = 8 \text{ fm}^{-1}$  the QMC method binds  ${}^4\text{He}$  more deeply by more than 1 MeV. In consequence, the extrapolated asymptotic values differ. Our results display a better convergence pattern with the cutoff. At the physical pion mass and with the same input observables, our highest-cutoff result is in good agreement with the highest-cutoff result (cutoff values in the range  $8\text{--}10 \text{ fm}^{-1}$ , but a different regulator function) of Ref. [15].

We found that an expansion of the type (3) up to  $1/\Lambda^2$  suffices to extrapolate the  ${}^4\text{He}$  energies for  $m_\pi = 140 \text{ MeV}$ , since the addition of a cubic term changes neither the extrapolated value nor the best-fit coefficients. For unphysical pion masses, the us-

age of the smallest cutoff is questionable because  $\Lambda = 2 \text{ fm}^{-1}$  cuts off momentum modes below the pion mass. We thus extrapolate the values appearing in the tables with the quadratic expansion in Eq. (3) but without the result at  $\Lambda = 2 \text{ fm}^{-1}$ . In all cases, we perform fits with and without the  $\Lambda = 2 \text{ fm}^{-1}$  results to estimate the systematic extrapolation error. The procedure adopted for the systematic and statistical errors quoted throughout this paper is detailed in the appendix.

It has to be remarked that this cutoff sensitivity study does not account for the EFT truncation error. Using cutoff variation from cutoff values somewhat larger than the pion mass, for example from  $\Lambda = 2 \text{ fm}^{-1}$ ,  $4 \text{ fm}^{-1}$ , and  $6 \text{ fm}^{-1}$  for  $m_\pi = 140, 510$ , and  $805 \text{ MeV}$ , we might estimate the error as  $\pm 7$ ,  $\pm 4$ , and  $\pm 30$ , respectively. Except for the intermediate pion mass, this is consistent with the rougher dimensional-analysis estimate  $Q_A/M \sim 0.3$ . In any case, we expect the truncation error to dominate over the statistical and extrapolation errors.

Given the convergence of the  ${}^4\text{He}$  binding energy with increasing cutoff, we confirm that, for both physical [15] and unphysical [7,9] pion masses, LO EFT( $\mathcal{N}$ ) is renormalized correctly without the need for a four-nucleon interaction. In the physical case, the binding energy is underestimated for all values of the cutoff we considered, but the extrapolated value is in agreement with experiment even if we neglect the truncation error. Of course when the latter is taken into account we must conclude that such a good agreement is somewhat fortuitous. We expect NLO corrections, including Coulomb and two-nucleon effective-range corrections, to change the result by a few MeV. For  $m_\pi = 510 \text{ MeV}$  and  $m_\pi = 805 \text{ MeV}$ , our results reproduce LQCD predictions (where Coulomb is absent) within the measurement error over the entire cutoff range. As pointed out in Refs. [7,9], this is a non-trivial consistency check: if either LQCD data or EFT( $\mathcal{N}$ ) were too wrong, one would expect no such agreement. However, LQCD uncertainties are too large at this point for us to draw a very strong conclusion.

It is interesting to study the cutoff dependence of the root-mean-square (rms) point-nucleon radius  $\sqrt{\langle r_{\text{pt}}^2 \rangle}$  and the single-nucleon point density  $\rho_{\text{pt}}(r)$ . These quantities are related to the charge density, which can be extracted from electron-nucleus scattering data, but are not observable themselves: few-body currents and single-nucleon electromagnetic form factors have to be accounted for. Still, one can gain some insight into the features of the ground-state wave function by comparing results at different pion masses and cutoffs. Since neither  $\sqrt{\langle r_{\text{pt}}^2 \rangle}$  nor  $\rho_{\text{pt}}(r)$  commute with the Hamiltonian, the desired expectation values on the ground-state wave function are computed by means of “mixed” matrix elements

$$\langle \Psi_0 | O | \Psi_0 \rangle \approx 2 \langle \Psi_T | O | \Psi_0 \rangle - \langle \Psi_T | O | \Psi_T \rangle. \quad (20)$$

In the above equation  $|\Psi_0\rangle$  is the imaginary-time evolved state of Eq. (4), while  $|\Psi_T\rangle$  is the trial wave function constructed as in Eq. (5).

The results for the point-proton radius of  ${}^4\text{He}$  are reported in Table 2. (Since Coulomb is absent in our calculation, the point-nucleon and point-proton radii are the same.) In the physical case, the calculated radius is much smaller than the empirical value – that is, the value extracted from the experimental data of Ref. [34] accounting for the nucleon size, but neglecting meson-exchange currents. A similar result,  $\sqrt{\langle r_{\text{pt}}^2 \rangle} \approx 1 \text{ fm}$  was obtained by the authors of Ref. [35] using a local form of a chiral interaction. NLO and  $\text{N}^2\text{LO}$  potentials in a chiral expansion based on naive dimensional analysis [3–5] bring theory into much closer agreement with the empirical value. Hence, sub-leading terms in the EFT( $\mathcal{N}$ ) expansion could play a relevant role, at least for physical values of the pion mass.

**Table 2**

${}^4\text{He}$  point-proton radius for different values of the pion mass  $m_\pi$  and the cutoff  $\Lambda$ , compared to the empirical value extracted from Ref. [34] accounting for the finite nucleon size. See main text and appendix for details on errors and extrapolations.

$\Lambda$	$m_\pi = 140 \text{ MeV}$	$m_\pi = 510 \text{ MeV}$	$m_\pi = 805 \text{ MeV}$
$2 \text{ fm}^{-1}$	$1.374 \pm 0.004$	$1.482 \pm 0.003$	$0.898 \pm 0.001$
$4 \text{ fm}^{-1}$	$1.203 \pm 0.004$	$1.133 \pm 0.003$	$0.699 \pm 0.001$
$6 \text{ fm}^{-1}$	$1.109 \pm 0.003$	$1.035 \pm 0.002$	$0.609 \pm 0.001$
$8 \text{ fm}^{-1}$	$1.054 \pm 0.003$	$0.976 \pm 0.001$	$0.542 \pm 0.001$
$\rightarrow \infty$	$0.9^{+0.008(\text{sys})}_{\pm 0.2(\text{stat})}$	$0.8^{+0.04(\text{sys})}_{\pm 0.1(\text{stat})}$	$0.25^{+0.05(\text{sys})}_{\pm 0.06(\text{stat})}$
“Exp.”	1.45	–	–

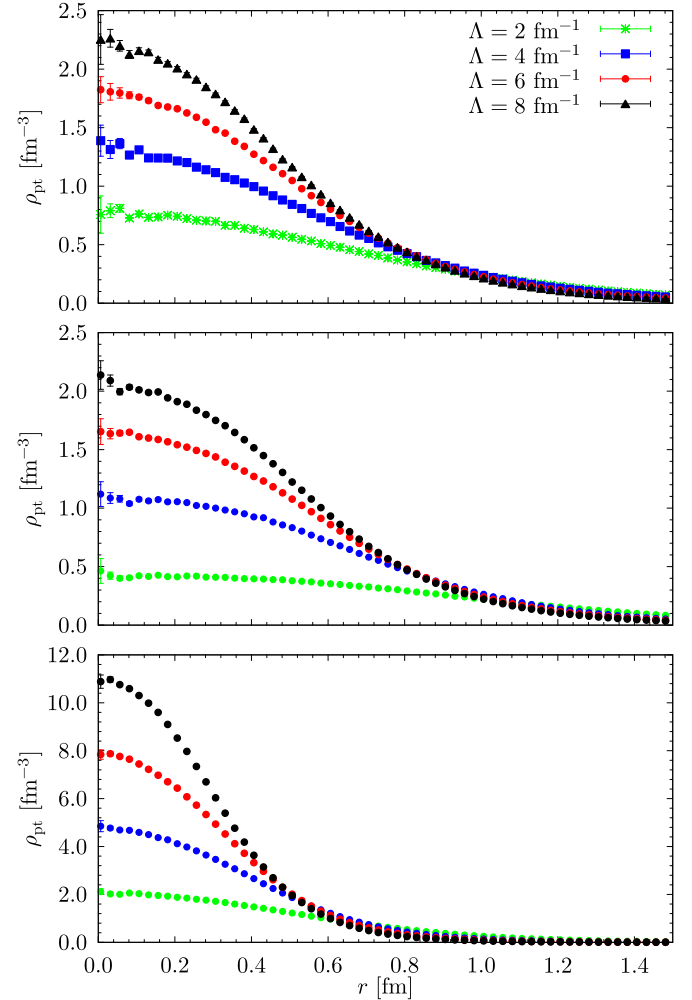


**Fig. 2.** (Color online)  ${}^4\text{He}$  single-nucleon point density for  $m_\pi = 140 \text{ MeV}$  (upper panel),  $m_\pi = 510 \text{ MeV}$  (middle panel), and  $m_\pi = 805 \text{ MeV}$  (lower panel), at different values of the cutoff  $\Lambda$ .

For unphysically large pion masses, where EFT( $\mathcal{N}$ ) is supposed to exhibit a faster convergence, the point-proton radius is smaller than at  $m_\pi = 140 \text{ MeV}$ . The value obtained for  $m_\pi = 510 \text{ MeV}$  indicates a spatial extent similar to the physical one, while  ${}^4\text{He}$  at  $m_\pi = 805 \text{ MeV}$ , in comparison, seems to be a much more compact object. This is consistent with the behavior of the single-nucleon point density,  $\rho_{\text{pt}}$ , displayed in Fig. 2. For all cutoff values, the density corresponding to  $m_\pi = 805 \text{ MeV}$  is appreciably narrower than that computed for  $m_\pi = 510 \text{ MeV}$  or  $m_\pi = 140 \text{ MeV}$ . Focusing on  $\Lambda = 8 \text{ fm}^{-1}$ ,  $\rho_{\text{pt}}$  has a maximum value of  $11.0 \text{ fm}^{-3}$  for  $m_\pi = 805 \text{ MeV}$ , while in the  $m_\pi = 510 \text{ MeV}$  and  $m_\pi = 140 \text{ MeV}$

**Table 3**

$^{16}\text{O}$  energy for different values of the pion mass  $m_\pi$  and the cutoff  $\Lambda$ , compared with experiment. (No LQCD data exist for this nucleus.) See main text and appendix for details on errors and extrapolations.

$\Lambda$	$m_\pi = 140$ MeV	$m_\pi = 510$ MeV	$m_\pi = 805$ MeV
$2 \text{ fm}^{-1}$	$-97.19 \pm 0.06$	$-116.59 \pm 0.08$	$-350.69 \pm 0.05$
$4 \text{ fm}^{-1}$	$-92.23 \pm 0.14$	$-137.15 \pm 0.15$	$-362.92 \pm 0.07$
$6 \text{ fm}^{-1}$	$-97.51 \pm 0.14$	$-143.84 \pm 0.17$	$-382.17 \pm 0.25$
$8 \text{ fm}^{-1}$	$-100.97 \pm 0.20$	$-146.37 \pm 0.27$	$-402.24 \pm 0.39$
$\rightarrow \infty$	$-115_{\pm 8}^{\pm 1(\text{sys})}$	$-151_{\pm 10}^{\pm 2(\text{sys})}$	$-504_{\pm 12}^{\pm 20(\text{sys})}$
Exp.	$-127.62$	-	-

cases the maximum values are  $2.1 \text{ fm}^{-3}$  and  $2.2 \text{ fm}^{-3}$ , respectively.

The similarity between  $^4\text{He}$  ground-state properties at  $m_\pi = 510$  MeV and those at the physical pion mass exists despite differences in the structure of lighter systems. If confirmed for other properties of  $^4\text{He}$  and heavier nuclei, this semblance would mean that simulations at intermediate pion masses could provide useful insights into the physical world while saving substantial computational resources.

In Table 3 the  $^{16}\text{O}$  ground-state energies are reported for the same pion-mass and cutoff values considered for  $^4\text{He}$ . A striking feature is that  $^{16}\text{O}$  is not stable against breakup into four  $^4\text{He}$  clusters in almost all the cases, the only exception occurring for  $m_\pi = 140$  MeV and  $\Lambda = 2 \text{ fm}^{-1}$ , where  $^{16}\text{O}$  is 4.5 MeV more bound than four  $^4\text{He}$  nuclei. In the other cases we miss the four- $^4\text{He}$  threshold by about 5 MeV, which is beyond our statistical errors and reveals a lower bound on the systematic error of our QMC method.

Even considering only statistical and extrapolation errors the asymptotic values of the  $^{16}\text{O}$  energy cannot be separated from the four- $^4\text{He}$  threshold. The proximity of the threshold suggests that the structure of our  $^{16}\text{O}$  should be clustered. Indeed, despite no explicit clustering being enforced in the trial wave function, the highly efficient optimization procedure arranges the two- and three-body Jastrow correlations, as well as the orbital radial functions, in such a way as to favor configurations characterized by four independent  $^4\text{He}$  clusters.

The single-proton density profiles displayed in Fig. 3 indicate that only for  $\Lambda = 2 \text{ fm}^{-1}$  with  $m_\pi = 140$  MeV and  $m_\pi = 510$  MeV are the nucleons distributed according to the classic picture of a bound wave function. For all the other combinations of pion masses and cutoffs, nucleons are pushed away from the center of the nucleus, which is basically empty – the density at the origin is a minuscule fraction of the peak – until  $\simeq 2$  fm from the center of mass. The erratic behavior of the peak position of the density profiles as a function of the cutoff has to be ascribed to the fact that the relative position of the four  $^4\text{He}$  clusters is practically unaffected by the cutoff value. In fact, once the clusters are sufficiently apart, a landscape of degenerate minima in the variational energy emerges. Hence, the single-proton densities correspond to wave functions that, despite potentially significantly different, lead to almost identical variational energies. In contrast, the width of the peaks decreases with increasing cutoff in step with the shrinking of the individual  $^4\text{He}$  clusters reported in Table 2.

The analysis of the proton densities alone does not suffice to support the claim of clustering. Another indication of clusterization comes from comparing the expectation values of the nuclear potentials evaluated in the ground states of  $^{16}\text{O}$  and  $^4\text{He}$ . For instance, in the  $m_\pi = 140$  MeV and  $\Lambda = 8 \text{ fm}^{-1}$  case it turns out that the expectation values of the  $^{16}\text{O}$  two- and three-body potentials are  $\simeq 4.05$  and  $\simeq 4.16$  times larger than the corresponding values for  $^4\text{He}$ . The same pattern is observed for all the combinations of pion mass and cutoff, except for  $\Lambda = 2 \text{ fm}^{-1}$  with

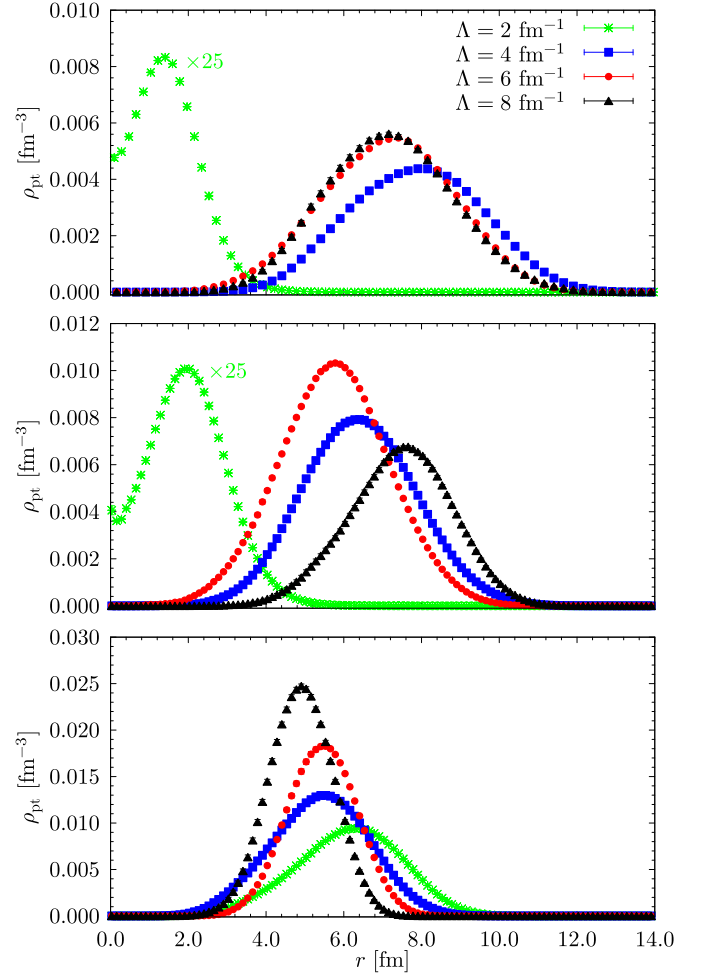


**Fig. 3.** (Color online)  $^{16}\text{O}$  single-nucleon point density for  $m_\pi = 140$  MeV (upper panel),  $m_\pi = 510$  MeV (middle panel), and  $m_\pi = 805$  MeV (lower panel), at different values of the cutoff  $\Lambda$ .

$m_\pi = 140$  MeV and  $m_\pi = 510$  MeV. In particular, for  $\Lambda = 2 \text{ fm}^{-1}$  and  $m_\pi = 140$  MeV, the expectation values of the two- and three-body potentials in  $^{16}\text{O}$  are  $\simeq 4.65$  and  $\simeq 6.14$  times larger than in  $^4\text{He}$ . This difference is a consequence of the fact that the number of interacting pairs and triplets is larger when clusterization does not take place.

To better visualize the clusterization of the wave function, in Fig. 4 we display the position of the nucleons following the propagation of a single walker for 5000 imaginary-time steps, corresponding to  $\Delta\tau = 0.125 \text{ MeV}^{-1}$ , printed every 10 steps. In the upper panel, concerning  $m_\pi = 140$  MeV and  $\Lambda = 2 \text{ fm}^{-1}$ , nucleons are not organized in clusters. In fact, during the imaginary-time propagation they diffuse in the region in which the corresponding single-nucleon density of Fig. 3 does not vanish. A completely different scenario takes place at the same pion mass when  $\Lambda = 8 \text{ fm}^{-1}$ : the nucleons forming the four  $^4\text{He}$  clusters remain close to the corresponding centers of mass during the entire imaginary-time propagation. This is clear evidence of clustering. It has to be noted that the relative position of the four clusters is not a tetrahedron. To prove this, for each configuration we computed the moment-of-inertia matrix as in Ref. [36]. If the  $^4\text{He}$  clusters were positioned at the vertices of a tetrahedron, diagonalization would yield only two independent eigenvalues. Instead, we found three distinct eigenvalues, corresponding to an ellipsoid – yet another indication of the absence of interactions among nucleons belonging to different  $^4\text{He}$  clusters.

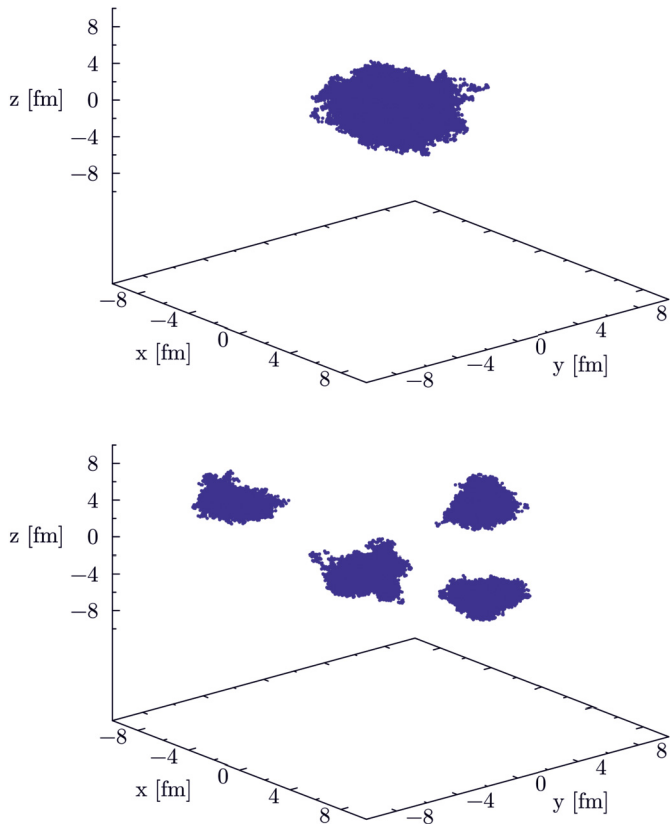


**Fig. 4.** (Color online) Imaginary-time diffusion with time step  $\Delta\tau = 0.125 \text{ MeV}^{-1}$  of a single walker for  $m_\pi = 140 \text{ MeV}$ , at  $\Lambda = 2 \text{ fm}^{-1}$  (upper panel) and  $\Lambda = 8 \text{ fm}^{-1}$  (lower panel).

The non-clustered states at  $\Lambda = 2 \text{ fm}^{-1}$  for  $m_\pi = 510 \text{ MeV}$  and  $m_\pi = 140 \text{ MeV}$  deserve further comment. The state at  $m_\pi = 510 \text{ MeV}$  stands in contrast to the other states found above threshold whose structure is clustered. We interpret this as an artifact of the numerical method, since a perfect optimization procedure should have produced a clustered structure resembling the lower-energy state with four free  ${}^4\text{He}$ . While there is no signal of  ${}^{16}\text{O}$  stability above the physical pion mass, the state at  $m_\pi = 140 \text{ MeV}$  is certainly stable at the lowest cutoff, that is, when the interaction has the longest range. On this basis, one might speculate that at some pion mass above the physical one a transition from a non-clustered to a clustered state is expected. However, such a conclusion cannot be drawn until higher-order calculations in EFT( $\mathcal{N}$ ) – which will capture finer effects from pion exchange such as the tensor force at  $\text{N}^2\text{LO}$  – are available.

The smaller relative size of the model space leads to more modest signs of cutoff convergence for  ${}^{16}\text{O}$  than  ${}^4\text{He}$ , which are reflected in larger extrapolation errors, especially at  $m_\pi = 805 \text{ MeV}$ . At physical pion mass, the central value of the extrapolated total energy is only 10% off experiment, which can be bridged by statistical and extrapolation errors. This difference is small compared to the expected truncation error,  $\sim 30\%$ . If there is a low-lying resonant or virtual state of  ${}^4\text{He}$  nuclei at LO in EFT( $\mathcal{N}$ ) – note that our analysis does neither preclude nor identify such a state – it is possible that the (perturbative) inclusion of higher-order terms up to  $\text{N}^2\text{LO}$  will move the  ${}^{16}\text{O}$  energy sufficiently for stability with respect to four  ${}^4\text{He}$  clusters.

For unphysical pion mass, our results can be seen as an extension of LQCD to medium-mass nuclei, with no further assumptions about the QCD dynamics. In this case, a determination of the rela-

tive position of the four- ${}^4\text{He}$  threshold would further require much increased accuracy in the  $A = 2, 3$  LQCD data that we use as input.

## 5. Conclusions

This paper represents the first application of the effective-field-theory formalism, as developed for small nuclei without explicit pions, to a relatively heavy object,  ${}^{16}\text{O}$ . We employed contact potentials which represent the leading order of a systematic expansion of QCD. This enabled us to analyze physical nucleons as well as simulated scenarios with increased quark masses.

To overcome the peculiar challenges associated with the solution of the Schrödinger equation, we have improved AFDMC by introducing a new optimization protocol of the many-body wave function to be employed in the variational stage of the calculation. The scheme we propose is an extension of the linear method and provides a much faster convergence in parameter space compared to stochastic reconfiguration, previously adopted in nuclear QMC calculations. Such accurate trial wave function is the starting point of the imaginary-time projection in AFDMC, which filters out the “exact” ground state of the Hamiltonian. This algorithm was used to predict not only ground-state energies, but also radii, densities, and particle distributions.

Our results for the  ${}^4\text{He}$  binding energy are in agreement with previous findings, including the renormalizability of the four-nucleon system in EFT( $\mathcal{N}$ ) without a LO four-body force. In particular, at physical pion mass the energy agrees with experiment within theoretical uncertainties. Moreover, the calculated point-nucleon radii and single-particle densities reveal a  ${}^4\text{He}$  structure at  $m_\pi = 510 \text{ MeV}$  similar to that at physical pion mass.

With this successful benchmark, we extended the calculations to  ${}^{16}\text{O}$ , obtaining extrapolated values for the  ${}^{16}\text{O}$  energy at all pion masses which are indistinguishable from the respective four- ${}^4\text{He}$  threshold, even considering only the smaller statistical and extrapolation errors. In fact, for almost all cutoffs and pion masses we considered,  ${}^{16}\text{O}$  is unstable with respect to break-up into four  ${}^4\text{He}$  nuclei. Our calculation of the  ${}^{16}\text{O}$  energy is the first time LQCD data are extended to the medium-mass region in a model-independent way.<sup>1</sup>

Interestingly,  $m_\pi = 140 \text{ MeV}$  and  $\Lambda = 2 \text{ fm}^{-1}$  is the only parameter set which yields a stable  ${}^{16}\text{O}$ . This suggests that the long-range structure of the interaction is deficient at larger cutoff values and might have to be corrected, e.g. via one-pion exchange, to guarantee the binding of heavier nuclei *at LO*. Alternatively, within a pionless framework, higher-order terms could act as perturbations to move  ${}^{16}\text{O}$  with respect to the four- ${}^4\text{He}$  threshold. At physical pion mass the central value of the total energy is just about 10% off experiment. This is only slightly larger than the statistical and extrapolation errors, and well within the  $\sim 30\%$  truncation error estimate. We cannot exclude the possibility that agreement with data will improve with order. A comprehensive study of the various subsystems of  ${}^{16}\text{O}$  – for example,  ${}^{12}\text{C}$ ,  ${}^8\text{Be}$ , and  ${}^4\text{He}$ - ${}^4\text{He}$  scattering – could determine whether a resonant or virtual shallow state at LO is transformed into a bound state by subleading interactions, thus elucidating the relation between clusterization and QCD.

Note that the tensor force does not appear to be indispensable for the deuteron or other light nuclei to be bound, or for

<sup>1</sup> As this manuscript was being concluded, a calculation of doubly magic nuclei appeared [37], where a two-body potential model obtained from LQCD data at  $m_\pi = 469 \text{ MeV}$  was solved with the Self-Consistent Green’s Function method. The widely different input data and method translate into much smaller  ${}^4\text{He}$  and  ${}^{16}\text{O}$  energies than our results. No clear sign is found for a  ${}^{16}\text{O}$  state below the  ${}^4\text{He}$  threshold.

$^{16}\text{O}$  to be stable against the breakup into four  $^4\text{He}$  nuclei. For instance, the Argonne  $v_4'$  interaction [38], which does not contain tensor terms, yields energies of  $-32.83 \pm 0.05$  MeV for  $^4\text{He}$  and  $-180.1 \pm 0.4$  MeV for  $^{16}\text{O}$  [39]. In EFT( $\mathcal{N}$ ) the tensor force is only an N<sup>2</sup>LO (typically 10%) effect, which is small for the deuteron [10]. At large pion masses the tensor component should remain perturbative. Before including a tensor term we need to account for NLO terms, which could play a role in the stability of  $^{16}\text{O}$ . One of the goals of calculating  $^{16}\text{O}$  in EFT( $\mathcal{N}$ ) is to assess which features of the nuclear interaction are essential for a description of nuclei, and which can be considered small effects.

In order to better appreciate the cluster nature of our solution for  $^{16}\text{O}$ , we have studied the radial nucleon density and the sampled probability density for the nucleons. In both cases the occurrence of clusterization is evident. From our results it is not possible to infer any significant correlation between the clusters, which once more confirms the extremely weak interaction among them within EFT( $\mathcal{N}$ ). We would like to point out that localization was not imposed in the wave function used to project out the ground state; rather, it spontaneously arises from the optimization procedure (despite the correlations being fully translationally invariant) and it is preserved by the subsequent imaginary-time projection.

Current QMC (AFDMC) results have now reached an accuracy level that allows for discussing the few-MeV energies involved in this class of phenomena, which are relevant for a deeper understanding of how the systematics in nuclear physics arises from QCD. Starting from LQCD data obtained for values of  $m_\pi$  smaller than the ones employed in this work, and yet larger than the physical one, would allow us to establish the threshold for which nuclei as large as  $^{16}\text{O}$  are stable against the breakup into four  $^4\text{He}$  clusters, if such a threshold exists. To perform this analysis, it is essential to include higher-order terms in the EFT( $\mathcal{N}$ ) interaction, possibly up to N<sup>2</sup>LO, where tensor contributions appear. This also requires a substantial improvement of the existing LQCD data on light nuclei, which, even for large  $m_\pi$ , are currently affected by statistical errors that do not allow for an effective constraint of the interaction parameters.

## Acknowledgements

We would like to thank N. Barnea, D. Gazit, G. Orlandini, and W. Leidemann for useful discussions about the subject of this paper. This research was conducted in the scope of the Laboratoire international associé (LIA) COLL-AGAIN and supported in part by the U.S. Department of Energy, Office of Science, Office of Nuclear Physics, under contracts DE-AC02-06CH11357 (A.L.) and DE-FG02-04ER41338 (U.v.K.), and by the European Union Research and Innovation program Horizon 2020 under grant No. 654002 (U.v.K.). The work of A.R. was supported by NSF Grant No. AST-1333607. J.K. acknowledges support by the NSF Grant No. PHY15-15738. Under an award of computer time provided by the INCITE program, this research used resources of the Argonne Leadership Computing Facility at Argonne National Laboratory, which is supported by the Office of Science of the U.S. Department of Energy under contract DE-AC02-06CH11357.

## Appendix A. Statistical and systematic error estimation

The procedure we adopted in order to estimate the error in the extrapolations performed in this work is as follows. We can distinguish between two sources of errors. The first is a systematic error corresponding to the choice of neglecting the next (cubic) order in the expansion Eq. (3) and of removing the initial data

point at  $\Lambda = 2 \text{ fm}^{-1}$ . The second is a statistical error coming from the uncertainties in the data used for the extrapolation.

The first kind of error is estimated by considering the maximum spread in three different extrapolations: two quadratic extrapolations obtained by either neglecting the results at  $\Lambda = 2 \text{ fm}^{-1}$  or by using all available data (the latter is included only if the reduced  $\chi^2$  is  $\approx 1$ ) and a cubic extrapolation that uses all data.

For the second type of error, it is convenient to write Eq. (3) as a simple quadratic form,

$$O_\Lambda = O + c_0\Gamma + c_1\Gamma^2 + \dots \quad (21)$$

where  $\Gamma = 1/\Lambda$ . Given that we have only three pairs  $(\Lambda, O_\Lambda)$ , it is straightforward to see that

$$c_1 = \frac{1}{\Gamma_2 - \Gamma_3} \left[ \frac{O_2 - O_1}{\Gamma_2 - \Gamma_1} - \frac{O_3 - O_1}{\Gamma_3 - \Gamma_1} \right] \quad (22)$$

together with

$$c_0 = \frac{O_3 - O_1}{\Gamma_3 - \Gamma_1} - (\Gamma_3 + \Gamma_1) c_1 \quad (23)$$

and

$$O = O_1 - c_0\Gamma_1 - c_1\Gamma_1^2. \quad (24)$$

At this point it is simple to estimate the errors by propagation of the measurement uncertainty. We have

$$\delta c_1 = \frac{1}{\Gamma_2 - \Gamma_3} \sqrt{\left[ \frac{\delta O_2^2 + \delta O_1^2}{(\Gamma_2 - \Gamma_1)^2} + \frac{\delta O_3^2 + \delta O_1^2}{(\Gamma_3 - \Gamma_1)^2} \right]} \quad (25)$$

and

$$\delta c_0 = \sqrt{\frac{\delta O_3^2 + \delta O_1^2}{(\Gamma_3 - \Gamma_1)^2} + (\Gamma_3 + \Gamma_1)^2 \delta c_1^2}, \quad (26)$$

and then finally

$$\delta O = \sqrt{\delta O_1^2 + \delta c_0^2 \Gamma_1^2 + \delta c_1^2 \Gamma_1^4}. \quad (27)$$

Both error estimates appear in the results reported in the main text.

## References

- [1] S.R. Beane, E. Chang, S.D. Cohen, W. Detmold, H.W. Lin, T.C. Luu, K. Orginos, A. Parreño, M.J. Savage, A. Walker-Loud, Light nuclei and hypernuclei from quantum chromodynamics in the limit of SU(3) flavor symmetry, *Phys. Rev. D* 87 (3) (2013) 034506, <http://dx.doi.org/10.1103/PhysRevD.87.034506>, arXiv:1206.5219.
- [2] T. Yamazaki, K.-i. Ishikawa, Y. Kuramashi, A. Ukawa, Helium nuclei, deuteron and dineutron in 2+1 flavor lattice QCD, *Phys. Rev. D* 86 (2012) 074514, <http://dx.doi.org/10.1103/PhysRevD.86.074514>, arXiv:1207.4277.
- [3] P.F. Bedaque, U. van Kolck, Effective field theory for few nucleon systems, *Annu. Rev. Nucl. Part. Sci.* 52 (2002) 339–396, <http://dx.doi.org/10.1146/annurev.nucl.52.050102.090637>, arXiv:nucl-th/0203055.
- [4] E. Epelbaum, H.-W. Hammer, U.-G. Meißner, Modern theory of nuclear forces, *Rev. Mod. Phys.* 81 (2009) 1773–1825, <http://dx.doi.org/10.1103/RevModPhys.81.1773>, arXiv:0811.1338.
- [5] R. Machleidt, D.R. Entem, Chiral effective field theory and nuclear forces, *Phys. Rep.* 503 (2011) 1–75, <http://dx.doi.org/10.1016/j.physrep.2011.02.001>, arXiv:1105.2919.
- [6] K.E. Schmidt, S. Fantoni, A quantum Monte Carlo method for nucleon systems, *Phys. Lett. B* 446 (1999) 99–103, [http://dx.doi.org/10.1016/S0370-2693\(98\)01522-6](http://dx.doi.org/10.1016/S0370-2693(98)01522-6).
- [7] N. Barnea, L. Contessi, D. Gazit, F. Pederiva, U. van Kolck, Effective field theory for lattice nuclei, *Phys. Rev. Lett.* 114 (5) (2015) 052501, <http://dx.doi.org/10.1103/PhysRevLett.114.052501>, arXiv:1311.4966.

- [8] S.R. Beane, E. Chang, W. Detmold, K. Orginos, A. Parreño, M.J. Savage, B.C. Tiburzi, Ab initio calculation of the  $np \rightarrow d\gamma$  radiative capture process, Phys. Rev. Lett. 115 (13) (2015) 132001, <http://dx.doi.org/10.1103/PhysRevLett.115.132001>, arXiv:1505.02422.
- [9] J. Kirscher, N. Barnea, D. Gazit, F. Pederiva, U. van Kolck, Spectra and scattering of light lattice nuclei from effective field theory, Phys. Rev. C 92 (5) (2015) 054002, <http://dx.doi.org/10.1103/PhysRevC.92.054002>, arXiv:1506.09048.
- [10] J.-W. Chen, G. Rupak, M.J. Savage, Nucleon–nucleon effective field theory without pions, Nucl. Phys. A 653 (1999) 386–412, [http://dx.doi.org/10.1016/S0375-9474\(99\)00298-5](http://dx.doi.org/10.1016/S0375-9474(99)00298-5), arXiv:nucl-th/9902056.
- [11] X. Kong, F. Raveland, Coulomb effects in low-energy proton–proton scattering, Nucl. Phys. A 665 (2000) 137–163, [http://dx.doi.org/10.1016/S0375-9474\(99\)00406-6](http://dx.doi.org/10.1016/S0375-9474(99)00406-6), arXiv:hep-ph/9903523.
- [12] J. Vanasse, Fully perturbative calculation of  $nd$  scattering to next-to-next-to-leading-order, Phys. Rev. C 88 (4) (2013) 044001, <http://dx.doi.org/10.1103/PhysRevC.88.044001>, arXiv:1305.0283.
- [13] S. König, H.W. Griefhammer, H.-W. Hammer, U. van Kolck, Effective theory of  $^3\text{H}$  and  $^3\text{He}$ , J. Phys. G 43 (5) (2016) 055106, <http://dx.doi.org/10.1088/0954-3899/43/5/055106>, arXiv:1508.05085.
- [14] J. Vanasse, Triton charge radius to next-to-next-to-leading order in pionless effective field theory, Phys. Rev. C 95 (2) (2017) 024002, <http://dx.doi.org/10.1103/PhysRevC.95.024002>, arXiv:1512.03805.
- [15] L. Platter, H.-W. Hammer, U.-G. Meißner, On the correlation between the binding energies of the triton and the alpha-particle, Phys. Lett. B 607 (2005) 254–258, <http://dx.doi.org/10.1016/j.physletb.2004.12.068>, arXiv:nucl-th/0409040.
- [16] I. Stetcu, B.R. Barrett, U. van Kolck, No-core shell model in an effective-field-theory framework, Phys. Lett. B 653 (2007) 358–362, <http://dx.doi.org/10.1016/j.physletb.2007.07.065>, arXiv:nucl-th/0609023.
- [17] H. Georgi, Effective field theory, Annu. Rev. Nucl. Part. Sci. 43 (1993) 209–252, <http://dx.doi.org/10.1146/annurev.ns.43.120193.001233>.
- [18] D.B. Kaplan, Effective field theories, in: Beyond the Standard Model 5. Proceedings, 5th Conference, Balholm, Norway, April 29–May 4, 1997, 1995, arXiv:nucl-th/9506035.
- [19] T. Iritani, et al., Mirage in temporal correlation functions for baryon–baryon interactions in lattice QCD, J. High Energy Phys. 10 (2016) 101, [http://dx.doi.org/10.1007/JHEP10\(2016\)101](http://dx.doi.org/10.1007/JHEP10(2016)101), arXiv:1607.06371.
- [20] E. Berkowitz, T. Kurth, A. Nicholson, B. Joo, E. Rinaldi, M. Strother, P.M. Vranas, A. Walker-Loud, Two-nucleon higher partial-wave scattering from lattice QCD, Phys. Lett. B 765 (2017) 285–292, <http://dx.doi.org/10.1016/j.physletb.2016.12.024>, arXiv:1508.00886.
- [21] T. Inoue, S. Aoki, T. Doi, T. Hatsuda, Y. Ikeda, N. Ishii, K. Murano, H. Nemura, K. Sasaki, Two-baryon potentials and H-dibaryon from 3-flavor lattice QCD simulations, Nucl. Phys. A 881 (2012) 28–43, <http://dx.doi.org/10.1016/j.nuclphysa.2012.02.008>, arXiv:1112.5926.
- [22] B. Bazak, M. Eliyahu, U. van Kolck, Effective field theory for few-boson systems, Phys. Rev. A 94 (5) (2016) 052502, <http://dx.doi.org/10.1103/PhysRevA.94.052502>, arXiv:1607.01509.
- [23] U. van Kolck, Effective field theory of short range forces, Nucl. Phys. A 645 (1999) 273–302, [http://dx.doi.org/10.1016/S0375-9474\(98\)00612-5](http://dx.doi.org/10.1016/S0375-9474(98)00612-5), arXiv:nucl-th/9808007.
- [24] P.F. Bedaque, H.-W. Hammer, U. van Kolck, Renormalization of the three-body system with short range interactions, Phys. Rev. Lett. 82 (1999) 463–467, <http://dx.doi.org/10.1103/PhysRevLett.82.463>, arXiv:nucl-th/9809025.
- [25] S. Binder, et al., Few-nucleon systems with state-of-the-art chiral nucleon–nucleon forces, Phys. Rev. C 93 (4) (2016) 044002, <http://dx.doi.org/10.1103/PhysRevC.93.044002>, arXiv:1505.07218.
- [26] J. Carlson, S. Gandolfi, F. Pederiva, S.C. Pieper, R. Schiavilla, K.E. Schmidt, R.B. Wiringa, Quantum Monte Carlo methods for nuclear physics, Rev. Mod. Phys. 87 (2015) 1067, <http://dx.doi.org/10.1103/RevModPhys.87.1067>, arXiv:1412.3081.
- [27] S. Gandolfi, A. Lovato, J. Carlson, K.E. Schmidt, From the lightest nuclei to the equation of state of asymmetric nuclear matter with realistic nuclear interactions, Phys. Rev. C 90 (6) (2014) 061306, <http://dx.doi.org/10.1103/PhysRevC.90.061306>, arXiv:1406.3388.
- [28] S. Sorella, Wave function optimization in the variational Monte Carlo method, Phys. Rev. B 71 (2005) 241103, <http://dx.doi.org/10.1103/PhysRevB.71.241103>, <http://link.aps.org/doi/10.1103/PhysRevB.71.241103>.
- [29] I.E. Lagaris, V.R. Pandharipande, Variational calculations of realistic models of nuclear matter, Nucl. Phys. A 359 (1981) 349–364, [http://dx.doi.org/10.1016/0375-9474\(81\)90241-4](http://dx.doi.org/10.1016/0375-9474(81)90241-4).
- [30] A. Arriaga, V.R. Pandharipande, R.B. Wiringa, Three body correlations in few body nuclei, Phys. Rev. C 52 (1995) 2362–2368, <http://dx.doi.org/10.1103/PhysRevC.52.2362>, arXiv:nucl-th/9506036.
- [31] J. Toulouse, C.J. Umrigar, Optimization of quantum Monte Carlo wave functions by energy minimization, J. Chem. Phys. 126 (8) (2007) 084102, <http://dx.doi.org/10.1063/1.2437215>, arXiv:physics/0701039.
- [32] C.J. Umrigar, C. Filippi, Energy and variance optimization of many-body wave functions, Phys. Rev. Lett. 94 (2005) 150201, <http://dx.doi.org/10.1103/PhysRevLett.94.150201>.
- [33] M.W. Lee, M. Mella, A.M. Rappe, Electronic quantum Monte Carlo calculations of atomic forces, vibrations, and anharmonicities, J. Chem. Phys. 122 (24) (2005) 244103, <http://dx.doi.org/10.1063/1.1924690>.
- [34] C.R. Ottermann, G. Kobschall, K. Maurer, K. Rohrich, C. Schmitt, V.H. Walther, Elastic electron scattering from  $^3\text{He}$  and  $^4\text{He}$ , Nucl. Phys. A 436 (1985) 688–698, [http://dx.doi.org/10.1016/0375-9474\(85\)90554-8](http://dx.doi.org/10.1016/0375-9474(85)90554-8).
- [35] J.E. Lynn, J. Carlson, E. Epelbaum, S. Gandolfi, A. Gezerlis, A. Schwenk, Quantum Monte Carlo calculations of light nuclei using chiral potentials, Phys. Rev. Lett. 113 (19) (2014) 192501, <http://dx.doi.org/10.1103/PhysRevLett.113.192501>, arXiv:1406.2787.
- [36] R.B. Wiringa, S.C. Pieper, J. Carlson, V.R. Pandharipande, Quantum Monte Carlo calculations of  $A = 8$  nuclei, Phys. Rev. C 62 (2000) 014001, <http://dx.doi.org/10.1103/PhysRevC.62.014001>, arXiv:nucl-th/0002022.
- [37] C. McIlroy, C. Barbieri, T. Inoue, T. Doi, T. Hatsuda, Doubly magic nuclei from lattice QCD forces at  $M_{PS} = 469 \text{ MeV}/c^2$ , arXiv:1701.02607.
- [38] R.B. Wiringa, S.C. Pieper, Evolution of nuclear spectra with nuclear forces, Phys. Rev. Lett. 89 (2002) 182501, <http://dx.doi.org/10.1103/PhysRevLett.89.182501>, arXiv:nucl-th/0207050.
- [39] F. Pederiva, F. Catalano, D. Lonardoni, A. Lovato, S. Gandolfi, New insights on the hyperon puzzle from quantum Monte Carlo calculations, in: Proceedings, Compact Stars in the QCD Phase Diagram IV (CSQCD IV), Prerow, Germany, September 26–30, 2014, 2015, arXiv:1506.04042, <http://inspirehep.net/record/1376031/files/arXiv:1506.04042.pdf>.